Optics & Laser Technology 74 (2015) 36–42

Contents lists available at ScienceDirect

Optics & Laser Technology

journal homepage: www.elsevier.com/locate/optlastec

Laser controlled melting of H12 hot-work tool steel with B_4C particles at the surface

B.S. Yilbas [a,*], F. Patel [a], C. Karatas [b]

[a] ME Department, King Fahd University of Petroleum & Minerals, Dhahran, Saudi Arabia
[b] Engineering College, Hacettepe University, Turkey

ARTICLE INFO

Article history:
Received 9 March 2015
Received in revised form
1 May 2015
Accepted 17 May 2015
Available online 5 June 2015

Keywords:
Hot-work tool steel
Laser melting
B_4C particles

ABSTRACT

Laser controlled melting of pre-prepared H12 hot-work tool steel surface is carried out. B_4C particles in the carbon film are located at the workpiece surface prior to the laser treatment process. Nitrogen at high pressure is used as an assisting gas during the laser melting. Morphological and metallurgical changes in the treated layer are examined using scanning electron microscope, energy dispersive spectroscopy, and X-ray diffraction. Microhardness of the treated surface is measured and the residual stress formed at the treated surface vicinity is obtained using the X-ray diffraction technique. It is found that a dense layer consisting of fine grains is formed at the treated surface. Microhardness of the treated surface improves significantly because of fine grains, nitride compounds formed at the surface and micro-stresses developed due to mismatched of thermal expansion coefficients of B_4C and the base material. The residual stress formed at the surface is suppressed by the self annealing effect of the initially formed laser scans.

1. Introduction

Laser surface treatment of metallic substrates has several advantages over the conventional treatment techniques. Some of these include precision of operation, shallow heat affected zone, short processing time, local treatment, and low cost. H12 hot-work tool steel has excellent impact toughness, good resistance to thermal fatigue cracking and it is widely used for hot tooling applications. The tribological properties of the alloy surface can be improved through laser controlled melting [1]. Although laser controlled melting provides fine grains and dense layer at the surface, thermal stress developed in the treated layer is high, which limits the practical application of the treated surface. The pre-treatment of the alloy surface enables to reduce the residual stress and improves the microhardness of the treated surface. In addition, hard particle injection at the surface during the laser treatment process is possible through preparation of the alloy surface prior to the laser treatment process. This improves considerably the surface hardness of the alloys [2–4]. However, due to the mismatch between the thermal expansion coefficients and the base alloy, micro-stresses can be formed in the near neighborhood of the particles, which contributed to the residual stresses formed in the treated layer. Consequently, investigation into metallurgical and morphological changes, and residual stress formed in the laser treated pre-prepared alloy surface becomes essential.

Considerable research studies were carried out to examine laser treatment of steel surfaces. Laser surface modification of hot-work tool steel was studied by Dobrzanski et al. [5]. Their findings revealed that fine grains and dendritic structures were formed in the laser remelted zone with the crystallization direction depended on the heat obstruction from the laser beam influenced zone. Laser surface hardening of hot-worked tool steel was investigated by Lee et al. [6]. They showed that the surface hardness of the alloy increased almost twice of the base material hardness after the laser treatment process. Surface roughness and wear behavior of laser treated tool steel was even examined by Kasman and Saklakoglu [7]. They indicated that friction coefficient and wear rate were affected by the process parameters in which case, average friction coefficient and wear rate increased with increase in laser pulsing frequency. The properties of laser alloyed tool steel surface were investigated by Bonek et al. [8]. They showed that the fine grain martensite structure was responsible for hardness increase at the treated surface. Laser melting of tool steel surface was examined by Majumdar et al. [9]. They indicated that microhardness of the treated surface improved. notably and nitride compounds were formed at the surface because of the high pressure assisting nitrogen gas. Laser surface modification of tool steel was studied by Brabazon et al. [10]. Their findings revealed that the hardness profile through the surface was related to the laser treatment conditions and resultant microstructure. Surface modification of tool steel under YAG laser irradiation was

* Corresponding author.
E-mail address: bsyilbas@kfupm.edu.sa (B.S. Yilbas).

http://dx.doi.org/10.1016/j.optlastec.2015.05.012
0030-3992/

investigated by SeDao et al. [11]. They showed that penetration depth of the microhardness varied greatly with the laser processing parameters. Discrete laser spot transformation hardening of tool steel was examined by Jiang et al. [12]. They indicated that the maximum diameter and depth of transformation hardening zones with no surface melting increased with the increase of laser pulse energy. Thermal stability of laser nitride iron and stainless steel by annealing treatments was studied by Carpene et al. [13]. They showed that stainless steel had good thermal stability for nitrogen upto 500 °C; however, a gradual decrease in nitrogen concentration was observed at elevated temperatures. Laser micro/nanostructuring of tool surface was examined by Kulkarni and Chang [14]. Their findings revealed that ripple patterns were generated at the laser treated surface and the average period of the ripples was approximately equal to the laser wavelength. Laser treatment of alumina surfaces was investigated by Yilbas and Ali [15]. They indicated that laser treatment improved the tribological properties of the surface due to the presence of the hard particles and nitride species formation. Laser surface heating and model studies were presented by Shuja and Yilbas [16,17]. They demonstrated that laser power intensity and scanning speed had significant effect on the temperature field in the irradiated region. Thermal stability of a laser treated die material for semi-solid metal forming was investigated by Aqida et al. [18]. They showed that rapid heating and cooling from the laser glazing process, a metallic glass layer was developed which exhibited an average microhardness of 900 HV. Thermal fatigue properties of laser treated steels was examined previously [19]. They indicated that carbides and oxides elements were detected on the sample surface after the thermal fatigue test.

Although laser treatment of tool steel surface was investigated previously, the main interest was laser gas assisted nitriding of the treated surfaces [1]. However, the influence of the hard particles, which are injected at the surface, on the hardness and microstructure of the treated layer was left obscure. Consequently, in the present study, laser gas assisted treatment of pre-prepared H12 hot-work tool steel surface is carried out. The tribological and morphological changes in the laser treated layer are examined using scanning electron microscope, optical microscope, energy dispersive spectroscopy, and X-ray diffraction. Microhardness of the treated surface is measured and the residual stress developed at the surface vicinity is obtained using the XRD technique.

2. Experimental

A carbon dioxide laser (LC-ALPHA III) in pulse mode was used in the laser treatment experiments. The focusing lens was used to obtain the focused laser beam diameter of 0.3 mm at the workpiece surface. Nitrogen assisting gas emerging from a conical nozzle and co-axial with the laser beam was used. In laser surface treatment experiments, several tests were conducted incorporating the different laser parameters. The optimum surface treatment conditions were assessed based on the combination of laser parameters resulting in the depth of treated layer of 40–50 μm and giving rise to defect and asperity free treated surface. Increasing laser power 10% results in high thermal stresses in the surface region, which in turn causes micro-crack formation at the surface; however, the proper selection of laser output power and laser scanning speed gives rise to crack free surface. This situation can be observed from Fig. 1, in which SEM micrographs of laser treated surfaces due to two different laser output power settings. The laser treatment parameters selected based on the optimum treatment conditions are given in Table 1.

The workpiece used was hot-work tool steel (H12) with the size of $10 \times 20 \times 2.5$ mm^3. The water soluble phenolic resin was mixed with 5% (wt) of B_4C powders and the mixture was applied by

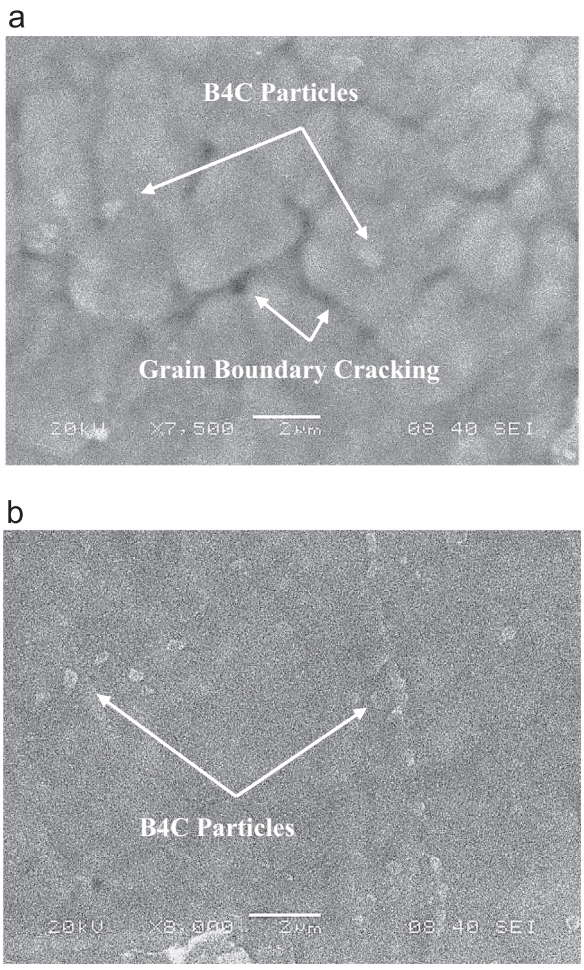

Fig. 1. Laser treated surface at two laser output power intensities. (a) Laser treated above 15% laser selected output power and (b) laser treated at the selected output power.

painting technique at the workpiece surface to form a layer with almost uniform thickness. The average powder size was 0.5 μm. Fig. 2 shows SEM micrograph of B_4C particles used in the experiments. With the multiple treatments in argon environment at 6 bar pressure in a furnace at temperature ranges 150–400 °C, the phenolic resin film was transformed into a carbon film accommodating 5% B_4C particles at the workpiece surface. It should be noted that almost uniform carbon layer was formed into a uniform film under the high pressure and temperature; in which case, pores formed in the carbon film, due to evaporation of water, was collapsed under the high pressure while resulting in almost uniform thickness carbon film. The pre-prepared workpiece surfaces were scanned by a laser beam according to the parameters given in Table 1.

A JEOL JDX-3530 Scanning Electron Microscope (SEM) was used to obtain micrographs of the cross-section of the workpieces after the tests. Energy Dispersive Spectroscopy (EDS) analysis was carried out at six different locations at the cross-section of the laser treated workpieces. The error related to the EDS analysis is estimated based on the repeatability of the data, which is on the order of 3%. A Bruker D8 Advance having CuKα radiation was used for X-ray Diffraction (XRD) analysis.

The residual stress formed at the surface vicinity of the laser treated workpiece was obtained using the XRD technique, since the position of the diffraction peak exhibits a shift as the specimen is rotated by an angle ψ. The relationship between the peak shift and the residual stress (σ) is given by [20]

Table 1
Laser heating conditions used in the experiment.

Scanning speed (cm/s)	Power (W)	Frequency (Hz)	Nozzle gap (mm)	Nozzle diameter (mm)	Focus setting (mm)	N_2 pressure (kPa)
10	85	1000	1.5	1.5	127	600

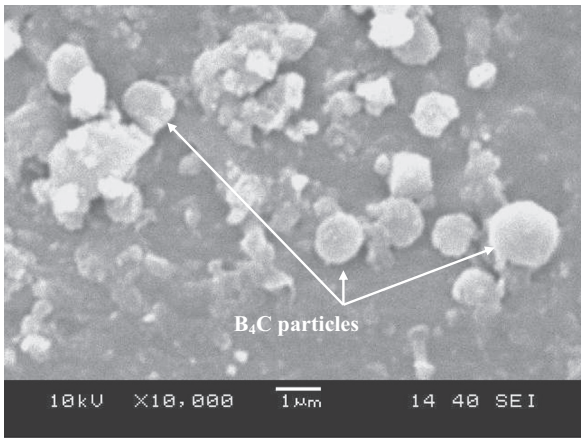

Fig. 2. SEM micrographs of B_4C particles used in the experiments.

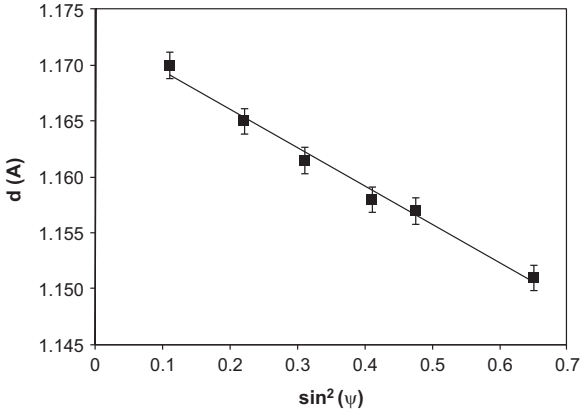

Fig. 3. Linear dependence of (211) with $\sin^2(\psi)$.

$$\sigma = \frac{E}{(1+\upsilon)\sin^2\psi}\frac{(d_n - d_0)}{d_0} \quad (1)$$

where E is Young's modulus, ν is Poisson's ratio, ψ is the tilt angle, and d_n are the d spacings measured at each tilt angle. If there are no shear strains present in the specimen, the d spacing changes linearly with $\sin^2\psi$. The bcc ferrite steel peak at (211) planes takes place at $2\theta = 88.3^\circ$ with the inter-planer spacing of 0.11709 nm. The linear dependence of $d(211)$ results in the slope of -3.27×10^{-13} m and the intercept of 1.17×10^{-10} m in Fig. 3. The residual stress determined is of the order of 480 ± 15 MPa. XRD measurements are repeated three times and the error related to the measurements is on the order of 3%. In addition, the coefficient of determination corresponding to the linear fit is $R^2 = 0.99$.

A Microphotonics digital microhardness tester (MP-100TC) was used to measure the microhardness at the surface of the nitride layer. The standard test method for Vickers indentation hardness of advanced ceramics (ASTM C1327-99) was adopted and a 300 g load was used during the tests. The measurements were repeated three times at each location at the surface and the error estimated is on the order of 5%.

A linear micro-scratch tester (MCTX-S/N: 01-04300) was used to determine the friction coefficient of the laser treated and untreated surfaces. The equipment was set at the contact load of 0.03 N and end load of 5 N. The scanning speed was 5 mm/min and loading rate was 5 N/s. The total length for the scratch tests was 5 mm.

3. Results and discussion

Laser treatment of pre-prepared hot-work tool steel surface is carried out. In the surface pre-preparation cycle, a carbon thin film is formed to accommodate B_4C particles uniformly at the surface. Analytical tools are used to characterize the laser treated surface and its cross-section. The residual stress formed at the surface vicinity is obtained using the XRD technique.

3.1. Morphological and metallurgical changes

Fig. 4 shows optical photographs and SEM micrographs of laser treated surface. It can be observed that the treated surface is free from large defect sites such as large cracks or crack networks. It should be noted that heat transfer from recently formed laser scanning tracks towards the early form tracks modifies the cooling rates. This, in turn, minimizes the thermally induced crack formation at the surface. Laser scanning tracks are distinguishable at the surface and they consist of overlapped laser spots. The close examination of the spots shows that overlapping ratio of the spots is on the order of 75%. It should be noted that laser heating at the surface took place with consecutive pulses with high reputation rate (1000 Hz). This results in overlapping of the irradiated spots at the workpiece surface. High magnification micrograph shows that partially embedded B_4C particles are present at the surface. This is associated with high melting temperature of B_4C. Since the melting at the surface is controlled to avoid evaporation at the surface, surface temperature of the workpiece remains within the neighborhood of the melting temperature of the substrate material. It should be noted that high laser pulse intensity results in excessive heating at the surface; in which case, surface evaporation is resulted and the cavity formation becomes unavoidable at the surface. The cavities produced, due to surface evaporation, increase the surface roughness and adversely affect the uniformity of the treated layer thickness. Since B_4C particles and the base material have different thermal expansion coefficients, microstresses are formed around B_4C particles after the completion of solidification. However, the close examination of the surface reveals that no microcrack or crack network is formed in the vicinity of B_4C particles at the treated surface. This indicates that the micro-stress levels formed at the surface are not high enough to initiate crack formation at the surface. Thermally induced stresses can cause the large crack formation at the surface due to high cooling rates, which covers the large area. However, the mismatch between the thermal expansion coefficients of B_4C and base alloy results in high strain in the near region of B_4C particles and the base alloy due to contraction during the solidification process. Therefore, micro-cracks or crack networks are expected to appear when the thermal strain due to this mismatch is high. The presence of crack free regions can be attributed to the self annealing effect of the previously formed laser scanning tracks. In this case, heat transfer from the previously formed tracks to the near region of B_4C particles suppresses the high solidification rates

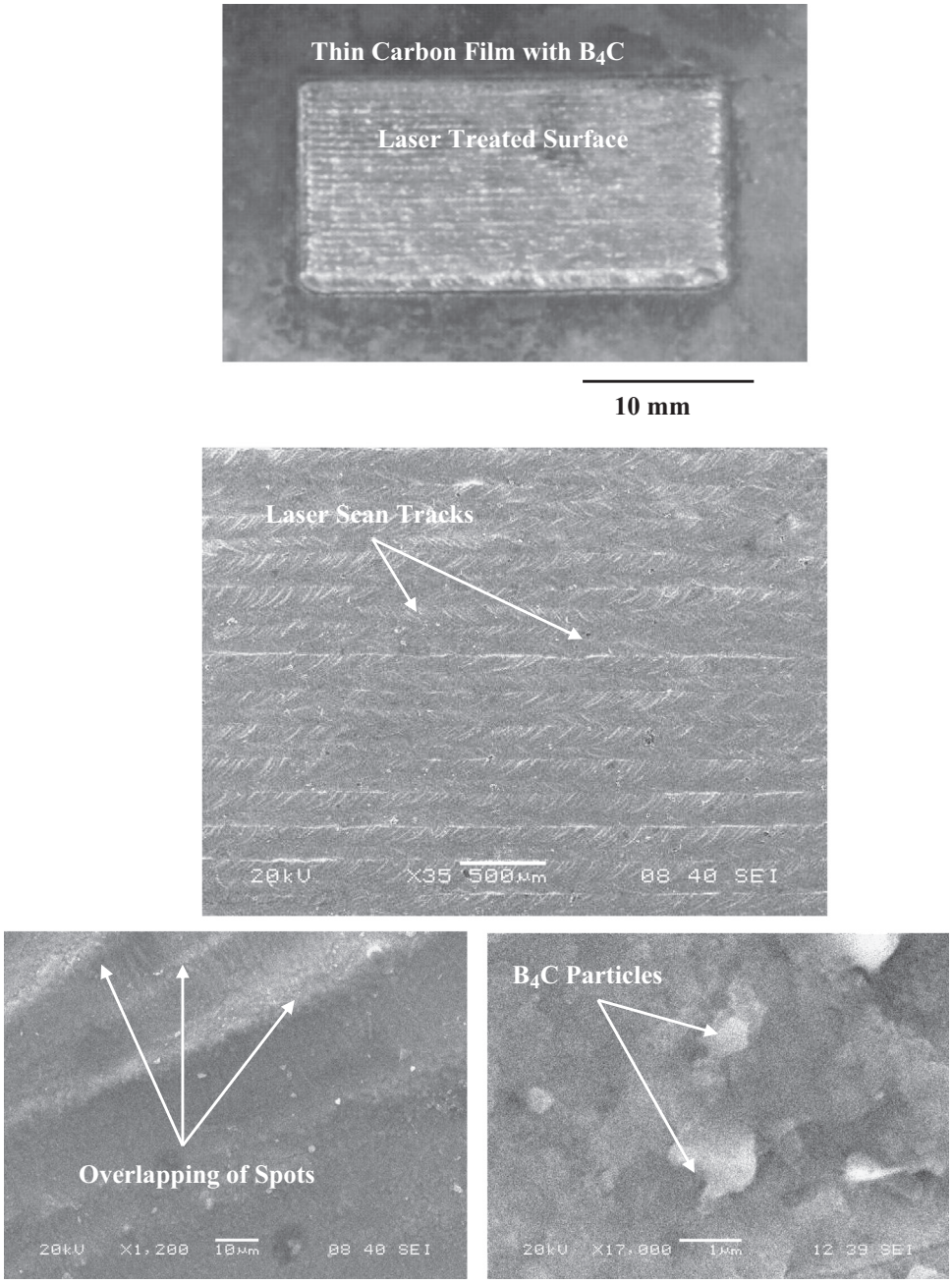

Fig. 4. Optical photograph and SEM micrographs of laser treated surface.

and lowers the micro-stress levels at the surface. Moreover, the surface is composed of fine grains indicating the high cooling rates. Although the solidification rate is slowed down due to self annealing effect, the cooling rate is high at the free surface. This is associated with the assisting gas, which enhances the convection cooling at the surface.

Fig. 5 shows the cross-section of the laser treated layer. The treated layer thickness extends almost uniformly 250 μm below the surface. This is attributed to the constant laser scanning speed at the surface. Three regions can be distinguished in the treated layer. In the first region, fine grains and dense layer is formed at the surface vicinity. In addition, randomly scattered B_4C particles are also evident in this region. The formation of fine grains and dense structure is because of the high cooling rates at the surface. Since nitrogen at high pressure is used at the surface, nitride compounds formed in the surface vicinity contributing to the formation of dense layer. This is because of the volume shrinkage at the surface vicinity leading to dense structure in this region. Moreover, no micro-crack is observed around B_4C particles due to mismatch of thermal expansion coefficient. However, few micro-voids are observed in the vicinity of the dense layer. This is attributed to volume shrinkage at the surface because of density variation. In the second region, which starts from the near vicinity of the dense layer, fine and closely spaced dendrites are formed. Since the cooling rates in this region is less than that at the surface, relative slow cooling rates is responsible for the formation of the closely spaced dendrites. However, the orientation of these dendrites is multi-directional, which indicates the non-uniform cooling in this region. The ferritic–pearlitic microstructure is transformed to a martensite in the dendritic spacing. As the depth below the surface increases further, the size of the dendrite increases and the cellular type structure is formed. This is attributed to relatively slow cooling rates in this region as compared to that

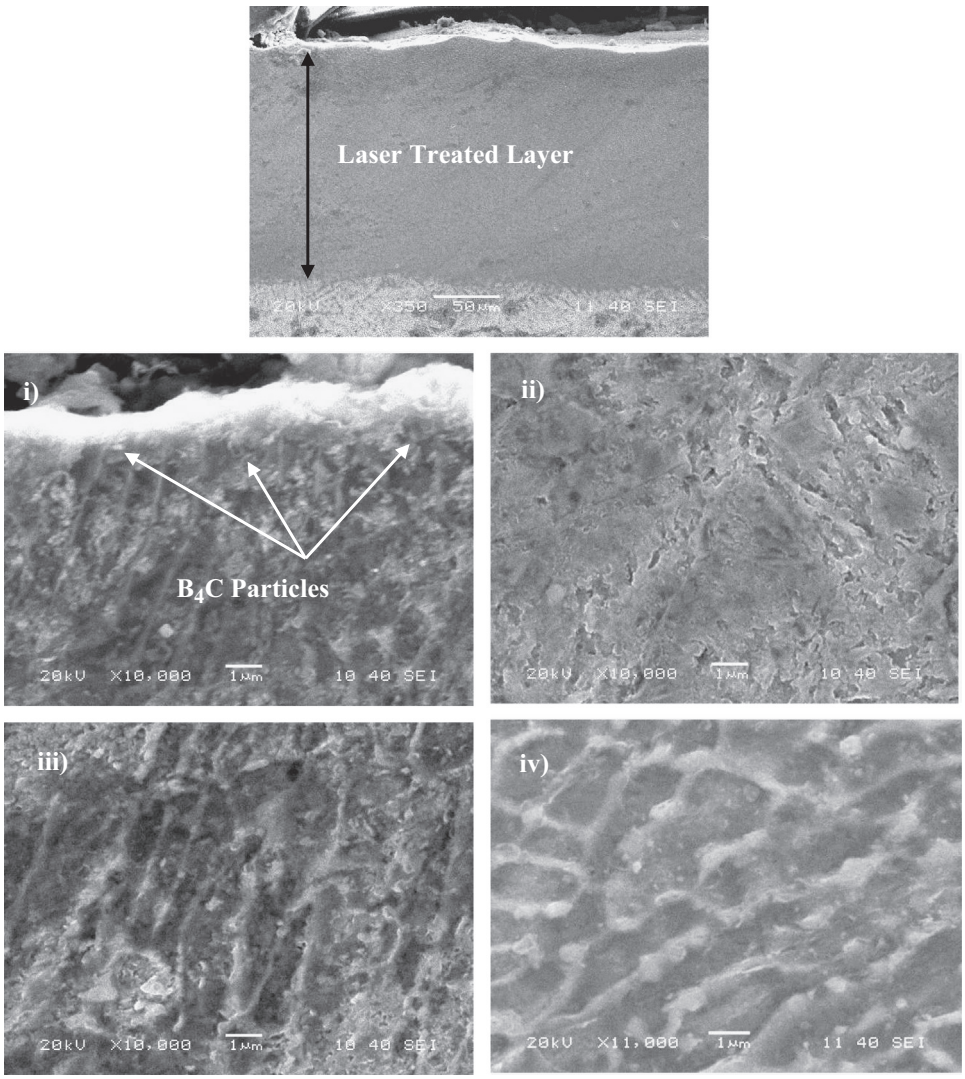

Fig. 5. SEM micrographs of laser treated layer: (i) fine grains and dense structure, (ii) feathery like structure, (iii) fine dendrites and (iv) cellular structure.

corresponding to the surface vicinity. The feathery like structures, which are formed in the close region of the surface, indicates the presence of nitrogen diffusion in this region. The use of high pressure nitrogen assisting gas is responsible for the formation of feathery like structures in this region. In the third region, grain coarsening is observed because of the slow cooling rates in this region. The demarcation line between the laser treated layer and the base material is visible. This is attributed to heat conduction from the treated layer to the base material, which influences the grain size in this region.

3.2. Composition, microhardness, residual stress, and scratch tests

Fig. 6 shows X-ray diffractorgram for the laser treated surface. The nitride peaks are evident form the diffractorgram. ε-Fe_2N and ε-Fe_3N peaks are the nitrogen rich compounds at the surface because of high pressure nitrogen assisting gas. However, γ'-Fe_4N peak corresponds to the precipitates below the surface. This results in feathery like structures below the dense layer, which is also evident from the SEM micrograph. The appearance of Fe_3(N, C) peaks in the diffractogram is associated with the carbon film formed at the surface prior to the laser treatment process. It should be noted that the position of Fe_3(N, C) peaks occurs at a less diffraction angle reference to ε-Fe_3N phase; consequently, the expansion of hcp lattice of Fe_3(N, C) phase took place. Moreover, the formation of CrN peaks

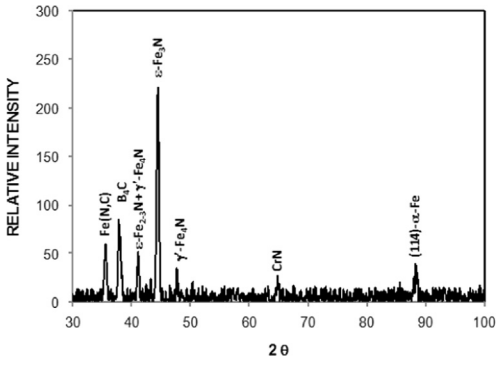

Fig. 6. X-ray diffractogram for laser treated surface.

in the diffractorgram is also observed, which is due to high pressure nitrogen assisting gas. Table 2 gives EDS data obtained at the surface. The change in elemental composition at the surface prior and after the laser treatment process is negligibly small, which indicates no partial evaporation takes place at the surface. Although quantification of light elements such as nitrogen in EDS data involves with error, the presence of nitrogen at the surface is evident. This indicates the formation of nitride compounds at the laser treated surface. Fig. 7 gives line scan of EDS data together with SEM image

Table 2
EDS data for laser treated surface (wt%).

Spectrum	N	Si	B	V	Cr	Mo	Fe
Spectrum 1	4.3	1.3	4.9	0.6	5.2	1.4	Balance
Spectrum 2	9.5	1.5	5.0	0.5	4.3	1.5	Balance
Spectrum 3	7.9	1.6	4.8	0.8	4.7	1.2	Balance
Spectrum 4	7.6	1.5	4.9	0.5	5.4	1.4	Balance

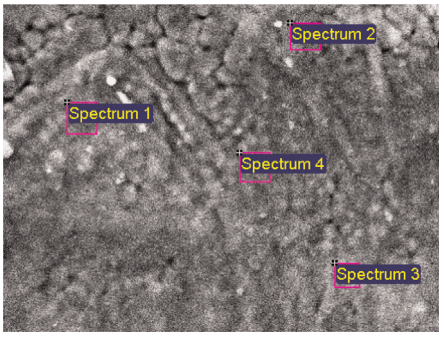

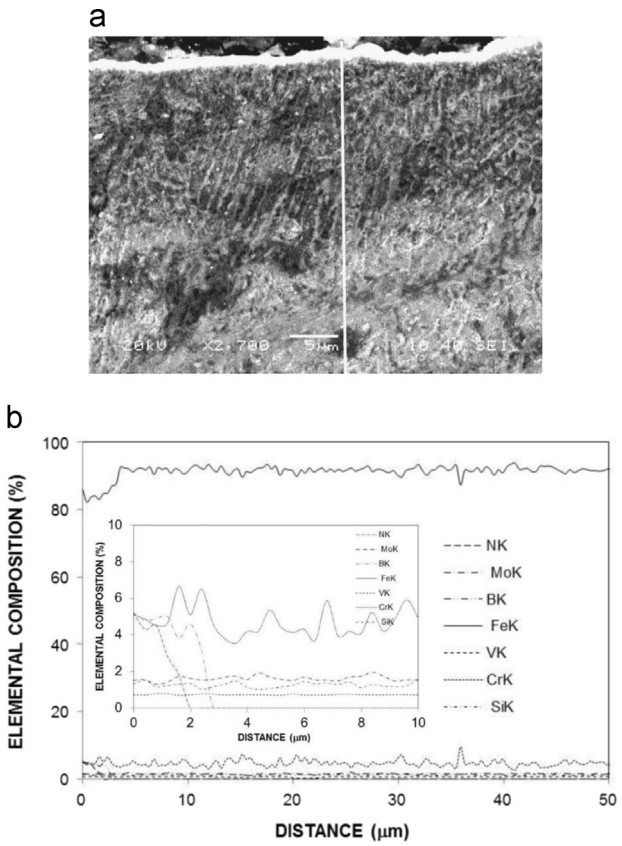

Fig. 7. EDS line scan across the cross-section of the laser treated layer. Small figure represents the elemental composition close to the laser treated surface (iron data is excluded to observe nitrogen and boron data): (a) SEM micrograph and (b) elemental distribution.

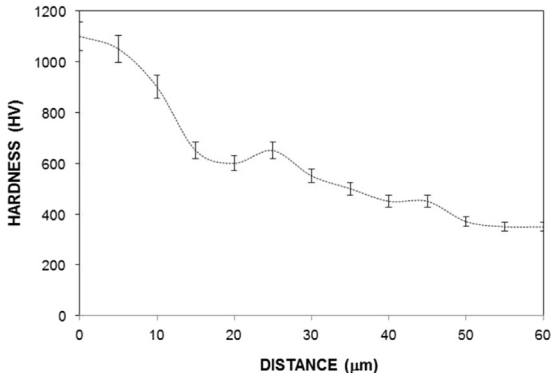

Fig. 8. Microhardness variation along the laser treated layer.

Table 3
Microhardness and residual stress obtained from XRD technique for the laser treated and untreated surfaces.

	Hardness (HV)	Residual stress (MPa)
As received	350 ± 10	–
Laser nitrided	850 ± 25	400 ± 15
Laser treated and B_4C	1100 ± 30	480 ± 15

where the line scan is carried out. Fig. 7 also contains the close view of the variation of the elemental composition of alloying elements, boron, and nitrogen in the laser treated surface region. It is evident that the depth of nitrogen is about 1.5 μm and boron is about 2.45 μm. Nitrogen reduces sharply in the surface region while boron remains almost constant. Consequently, the depth of nitrogen diffusion is limited with the surface region and mixing of B_4C particles with the base alloy takes place in the shallow depth of the laser treated layer. Fig. 8 shows microhardness depth distribution across the laser treated layer. Microhardness attains the maximum value in the surface region where B_4C particles are concentrated. As the depth below the surface increases, microhardness reduces first sharply and, then, the decay becomes gradual. Table 3 gives the microhardness of laser treated and untreated surfaces as well as the residual stress formed at the surface vicinity of the laser treated layer. It is evident that the microhardness increases significantly for the laser treated surface. This is attributed to one or all of the followings: (i) dense layer with the grains formed at the surface vicinity because of the high cooling rates at the surface, (ii) nitride compounds formed at the surface due to high pressure nitrogen assisting gas and (iii) microstresses formed in the near region of B_4C particles because of the mismatch of thermal expansion coefficients. The residual stress formed is on the order of -480 ± 15 MPa. It should be noted that the self annealing effect of the initially scan laser tracks reduces the residual stress at the surface.

Fig. 9 shows friction coefficient of the laser treated surfaces (Fig. 9a) and the scar marks (Fig. 9b) resulted during the scratch tests. Since the friction coefficient of the as received tool steel is 0.60 ± 0.045 [21], laser treatment lowers the friction coefficient at the surface. This is associated with reduced surface roughness and enhancement of surface microhardness after the laser treatment process. The close examination of the scratch images shows that the scar size is almost uniform and no crack around the scar mark

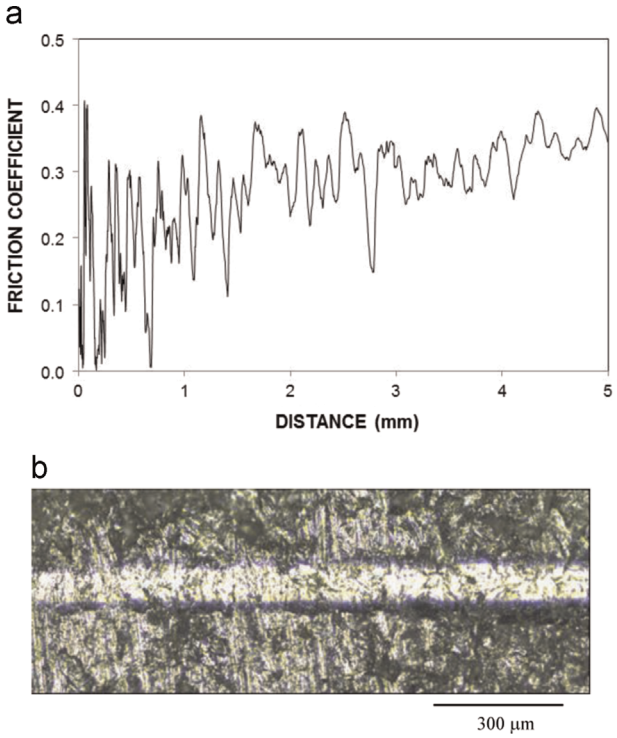

Fig. 9. Friction coefficient and scratch mark for laser treated layer. (a) Friction coefficient along the laser treated surface and (b) scratch mark resulted after the tests.

is observed. This indicates that the surface fracture toughness reduction due to surface hardness enhancement is not significant.

4. Conclusion

Laser treatment of pre-prepared H12 hot-work tool steel surface is carried out. A carbon film containing 5% B_4C particles is formed prior to the laser treatment process. Morphological and metallurgical changes in the laser treated layer are examined using scanning electron microscopy, energy dispersive spectroscopy, and X-ray diffraction. Microhardness of the treated surface is measured and the residual stress formed at the surface is obtained using the XRD technique. It is found that a dense layer consisting of fine grains formed at the treated surface. Imbedded B_4C articles are observed at the surface due to the controlled melting, in which case excessively high temperature heating at the surface is avoided during the treatment process. The specific conclusions derived from the present work can be listed as follows:

1. The treated surface is free from large asperities and defects. Although thermal expansion coefficients of B_4C and the base material are different, no micro-crack or crack-network is observed in the close region of B_4C particles. Formation of nitride compounds and the formation of dense layer at the surface results in volume shrinkage in the vicinity of the dense layer. This causes few and randomly scattered micro-voids in this region.
2. Small size dendritic structures are formed below the dense layer and as the depth below the surface increases; cellular structure is formed in the treated layer. Nitrogen diffusion through the grain boundaries results in the formation of γ'-Fe_4N compound below the surface.
3. The presence of carbon film and high pressure nitrogen assisting gas cause the formation of $Fe_3(C, N)$ compounds at the surface, which contribute significantly to hardness increase at the surface.
4. Microhardness of the treated layer increases notably due to the formation of nitride compound, fine grains, and micro-stresses formed in the near region of B_4C particles.
5. The residual stress determined is of the order of -480 ± 15 MPa, which is compressive. The self annealing effect of the initially formed tracks suppressed the residual stress levels at the surface.
6. Laser treatment reduces the friction coefficient of the surface.

Acknowledgments

The authors acknowledge the support of King Fahd University of Petroleum and Minerals, Dhahran, Saudi Arabia (Project no. SB131007) for this work.

References

[1] Yilbas BS, Ali H. Laser treatment of alumina surface with chemically distinct carbide particles. Opt Laser Technol 2014;64:1–6.
[2] Yilbas BS, Karatas C, Karakoc H, Abdul Aleem BJ, Khan S, Al-Aqeeli N. Laser surface treatment of aluminum based composite mixed with B_4C particles. Opt Laser Technol 2014;66:129–37.
[3] Yilbas BS, Karatas C, Arif AFM, Abdul Aleem BJ. Laser control melting of alumina surfaces and thermal stress analysis. Opt Laser Technol 2011;43(4):858–65.
[4] Yilbas BS, Akhtar S, Karatas C, Chatwin C. Laser embedding of TiC particles into the surface of phosphor bronze. Surf Interface Anal 2012;44(7):831–6.
[5] Dobrzanski LA, Bonek M, Piec M, Jonda E. Diode laser modification of surface gradient layer properties of a hot-work tool steel. Mater Sci Forum 2006;532–533:657–60.
[6] Lee J, Jang J, Joo B, Son Y, Moon Y. Laser surface hardening of AISI H13 tool steel. Trans Nonferr Met Soc China 2009;19(4):917–20.
[7] Kasman S, Saklakoglu IE. Surface roughness and wear behavior of laser machined AISI H13 tool steel. Adv Mater Res 2011;264–265:1264–9.
[8] Bonek M, Dobrzanski LA, Hajduczek E, Klimpel A. Structure and properties of laser alloyed surface layers on the hot-work tool steel. J Mater Process Technol 2006;175(1–3):45–54.
[9] Majumdar DJ, Nath AK, Manna I. Studies on laser surface melting of tool steel – Part II: mechanical properties of the surface. Surf Coat Technol 2010;204(9–10):1326–9.
[10] Brabazon D, Naher S, Biggs P. Laser surface modification of tool steel for semi-solid steel forming. Diffu Defect Data Part B: Solid State Phenom 2008;141–143:255–60.
[11] SeDao 1 HM, Hua M, Shao TM, Tam HY. Surface modification of DF-2 tool steel under the scan of a YAG laser in continuously moving mode. J Mater Process Technol 2009;209(10):4689–97.
[12] Jiang J, Xue L, Wang S. Discrete laser spot transformation hardening of AISI O1 tool steel using pulsed Nd:YAG laser. Surf Coat Technol 2011;205(21–22):5156–64.
[13] Carpene E, Landry F, Meng H, Lieb KP, Schaaf P. Investigation of the thermal stability of laser nitrided iron and stainless steel by annealing treatments. Hyperfine Interact 2002;139–140(1–4):355–61.
[14] Kulkarni K, Chang Z, Lei S. Surface micro/nanostructuring of cutting tool materials by femtosecond laser. Trans North Am Manuf Res Inst SME 2004;32:25–32.
[15] Yilbas BS, Ali H. Laser treatment of alumina surface with chemically distinct carbide particles. Opt Laser Technol 2014;64:1–6.
[16] Shuja SZ, Yilbas BS. Laser heating of a moving slab: influence pulse intensity parameter on temperature and stress fields. Opt Laser Technol 2015;70:7–16.
[17] Shuja SZ, Yilbas BS. Laser induced heating of coated carbon steel sheets: consideration of melting and marangoni flow. Opt Laser Technol 2013;47:47–55.
[18] Aqida SN, Maurel M, Brabazon D, Naher S, Rosso M. Thermal stability of laser treated die material for semi-solid metal forming. Int J Mater Form 2009;2 (Suppl. 1):S761–4.
[19] Aqida SN, Calosso F, Brabazon D, Naher S, Rosso M. Thermal fatigue properties of laser treated steels. Int J Mater Form 2010;3(Suppl. 1):S797–800.
[20] Khana ZA, Hadfield M, Tobe S, Wang Y. Ceramic rolling elements with ring crack defects – a residual stress approach. Mater Sci Eng A 26, 2005;404:221–2.
[21] Barrau O, Boher C, Vergne C, Rezai-Aria F. Investigations of friction and wear mechanisms of hot forging tool steels. In: Proceedings of the 6th international tooling conference. Karlstad University, Sweden; 10–13 September 2002, p. 95–111.